Ukrainian Journal of Physical Optics
ISSUE 1
2027

ENERGY-EFFICIENCY COMPARISON OF ELECTRIC- AND MAGNETIC-FIELD ENHANCEMENT OF ACOUSTO-OPTIC DIFFRACTION IN $PbMoO_4$ CRYSTALS

O. MYS, M. KOSTYRKO, I. SKAB, R. VLOKH*

O.G. Vlokh Institute of Physical Optics of the Ivan Franko National University of Lviv,
23 Dragomanov Str., 79005, Lviv, Ukraine
*Corresponding author: vlokh@ifo.lviv.ua

Received: 12.09.2026

Abstract. This work considers the influence of electric and magnetic fields on the acousto-optic (AO) figure of merit in $PbMoO_4$ crystals, arising from electro-gyration and Faraday effects that induce elliptical birefringence. A few types of anisotropic AO interactions with the slowest acoustic wave QT_1 were analyzed: collinear forward and backward AO diffraction and tangential forward and backward AO diffraction. The highest AO figure of merit (29×10^{-15} s^3/kg) is achieved with backward tangential AO diffraction at E_3^0 =10^8 V/m (or magnetic field 795.8 kA/m). It has been found that even at E_3^0 =10^6 V/m (or magnetic field 37.5 kA/m), the AO figure of merit increases to 23×10^{-15} s^3/kg, i.e., the AO figure of merit increases by a factor of 2.3 under electric or magnetic field application. For this case of AO diffraction, a comparative analysis of the energy densities of the electric and magnetic fields required to enhance AO diffraction efficiency to a certain level by increasing the AO figure of merit and the power of the acoustic wave, which is necessary to achieve this AO efficiency without applying an electric or magnetic field, has been carried out. It has been found that with the chosen parameters, the electric and magnetic field energy densities are much higher than those of the acoustic wave. Nonetheless, there are many conditions under which these energy densities can be equalized.

Keywords: acousto-optic diffraction, electro-gyration, Faraday effect, acousto-optic efficiency, energy density

UDC: 535.42:534, 535.568, 535.016
DOI: 10.3116/16091833/Ukr.J.Phys.Opt.2027.01077
This work is licensed under the Creative Commons Attribution International License (CC BY 4.0).

1. Introduction

Acousto-optic (AO) diffraction involves the interaction of optical waves with a dielectric permeability grating in a medium, created by an acoustic wave (AW) through the elasto-optic (EO) effect [1-3]. It is one of the most intriguing and commonly employed parametric optical effects, alongside Pockels, Kerr, piezo-optic, Faraday, and electro-gyration effects [4]. AO diffraction enables various applications, such as modulating light intensity by adjusting the AW amplitude, steering a light beam through AO frequency tuning, and altering light polarization via anisotropic AO diffraction. Consequently, AO diffraction plays a central role in many optoelectronic devices, including AO tunable filters [5], AO modulators, Q-switches, and RF spectrum analyzers [6]. Recently, AO control of optical radiation has extended to emerging fields, such as microparticle manipulation with optical beams [7], targeting optical beams with different quantum states in quantum cryptography and optical computing [8,9], and the creation of Bose-Einstein condensates [10].

A key feature of AO Bragg diffraction is the AO figure of merit, which measures the diffraction efficiency - the fraction of optical intensity directed into the diffraction maximum. The diffraction efficiency in AO Bragg diffraction is given by the following relation:

$$\eta = I / I_0 = \sin^2\left(\frac{\pi}{\lambda \cos\theta_B} \sqrt{M_2 P_a \frac{l}{2b}} \right), \quad (1)$$

where I and I_0 are the intensities of the diffracted and incident light, respectively. λ is the wavelength of optical radiation, θ_B is the Bragg angle, P_a is the AW power, M_2 is the AO figure of merit, l is the interaction length, and b is the height of the acoustic beam. In its turn, the M_2 factor is determined as

$$M_2 = \frac{n_i^3 n_d^3 p_{eff}^2}{\rho v_{kl}^3}. \quad (2)$$

In this context, n_i and n_d represent the refractive indices of the incident and diffracted waves, respectively p_{eff} is the effective EO coefficient, ρ the material density, and v_{kl} is the AW velocity. The indices k and l denote the propagation and polarization directions of the AW. As shown in Eq. (2), the AO figure of merit depends on several constitutive parameters, most of which are tensor quantities. Their structure and the number of non-zero components depend on the medium's symmetry. For example, AW velocities are calculated via the Christoffel equation, utilizing a fourth-rank elastic-stiffness tensor $C_{\lambda\mu}$ [Note: Greek indices follow Voigt notation]. The effective EO coefficients result from complex relations involving components of a fourth-rank EO tensor $p_{\lambda\mu}$, while the refractive indices are derived from a second-rank impermeability tensor B_μ [11]. The AO figure of merit is highly influenced by the slowness of the AW involved in AO interactions. A slower wave increases the figure of merit but increases rise times. To improve the AO figure of merit, selecting materials with higher effective EO coefficients is advisable. Typically, EO tensor components do not exceed 0.4 at standard conditions [12], meaning the effective EO coefficient is of similar magnitude. Thus, the AO figure of merit usually reaches only a few tens, with a factor of 10^{-15} s^3/kg. This often proves insufficient for many applications.

The effect of optical activity can increase the AO figure of merit. For the first time, this was shown in the work [13], where accounting for natural optical rotation led to doubling the AO figure of merit in TeO_2 crystals from ~600×10^{-15} s^3/kg for interacting linearly polarized optical waves with a quasi-transverse AW to ~1200×10^{-15} s^3/kg for the case of interacting circularly polarized optical waves with the same AW. As shown in a number of our recent works (see e.g. [14,15]), removing the circular birefringence degeneracy can substantially enhance the AO figure of merit when the incident optical wave's polarization coincides with the eigenwave participating in the AO interaction. This occurs because the square of the eigenwave's ellipticity becomes an additional term in the effective EO coefficient, multiplied by additional components of the EO tensor. It has also been demonstrated that, in this context, not only natural optical activity but also induced optical activity can be used. These include electro-gyration [16] and the Faraday effect [17,18].

Note that although electro-gyration, resulting from spatial dispersion, differs from the Faraday effect, caused by the magnetic field's time-reversal symmetry, both can be utilized together in optical devices. A bright example of such utilization is the magneto-optic sensor, which is based on electro-gyration compensation for the Faraday rotation [19]. This device can measure both electric and magnetic fields by Faraday and electro-gyration compensation of the induced optical rotation, respectively. The device has been based on the use of $PbMoO_4$ crystals, which are highly efficient electro-gyration materials (the electro-gyration coefficient is equal to $\beta_{33}=(1.23\pm0.12)\times10^{-12}$m/V (λ=517 nm) [20]). The Verdet constant for lead-molybdate crystals is

not the highest one among magnetically non-ordered materials and is equal to V=(6.5±0.2)×10^{-5} rad/A (λ=635 nm) [21]. The correspondence between electric field strength (E_3^0) and magnetic flux density (B_3^0) or magnetic field strength (H_3^0) is as follows: $E_3^0 / B_3^0 \approx 2.02\times10^7$ V/m×T or E_3^0 / H_3^0 =25.4 V/A. Therefore, for the compensation of electro-gyration optical rotation induced by the magnetic field of 1 A/m it is necessary to apply an electric field of 25.4 V/m.

It should be noted that in our work [15], we have experimentally demonstrated modulation of the intensity of the diffracted optical wave in TeO_2 crystals by externally modulating the ellipticity of the incident optical wave. This effect arises from circular (elliptical) birefringence due to natural optical activity and its influence on the efficiency of AO diffraction. Obviously, the application of magnetic and electric fields increases the degrees of freedom for the operation of refractive index degeneracy and, as a result, increases the possibility of AO operation of optical radiation. In the present work, we analyze the influence of both magnetic and electric fields on the efficiency of AO diffraction in the non-ferromagnetic and non-ferroelectric lead molybdate crystal. This work compares the energy densities of enhancing AO efficiency using magnetic and electric fields with those of increasing AW power.

2. Method of analysis

The $PbMoO_4$ crystals belong to the point group of symmetry 4/m [22]. The fundamental absorption edge corresponds to a wavelength of 378 nm [23]. In the IR spectral range, these crystals manifest triplet absorption bands centered at about 4039, 4233, and 4460 nm [23]. The electro-gyration coefficient calculated from the data [20] for λ=632.8 nm is equal to β_{33}=(1.17±0.12)×10^{-12}m/V. The Verdet constant has been taken for the wavelength of 635 nm [21]. The refractive indices are equal: n_o=2.386, and n_e= 2.262 (λ=632.8 nm) [24]. From the same source, we have taken the elastic stiffness coefficients and components of the EO tensor. They are equal p_{11}=0.24, p_{33}=0.300, p_{l2}=0.24, p_{l3}=0.255, p_{l6}=0.017, p_{31}=0.175, p_{44} =0.067, p_{45}= -0.01, p_{61}=0.013, p_{66}=0.05, and C_{11} = 109.2, C_{l2}=68.3, C_{13}=52.8, C_{16}=l3.6, C_{33}=91.7, C_{44}=26.7, C_{66}=33.7 GPa, respectively. The material density is equal to ρ=6950 kg/m^3.

To reach conditions with a high value of the eigenwaves' ellipticity, which corresponds to the incident optical waves, these waves have to propagate close to the optical axis (*Z*-axis, which corresponds to the *c* crystallographic axis). Therefore, the AW has to propagate close to the *XY* plane (*ab*–crystallographic plane). In order to find the parameters of the slowest AW that propagates in the *XY* plane, we have calculated the AW's velocity contours on the basis of the Christoffel equation and the data of the elastic stiffness tensor components with using of relations:

$$v_{QT_1} = \sqrt{\frac{C_{11}+C_{66}}{2\rho} - \frac{\sqrt{(C_{11}-C_{66})^2\cos^2 2\varphi + 4(C_{16}\cos 2\varphi + 0.5(C_{12}+C_{66})\sin 2\varphi)^2}}{2\rho}},$$
$$v_{PT_2} = \sqrt{\frac{C_{44}}{\rho}}, \qquad (3)$$
$$v_{QL} = \sqrt{\frac{C_{11}+C_{66}}{2\rho} + \frac{\sqrt{(C_{11}-C_{66})^2\cos^2 2\varphi + 4(C_{16}\cos 2\varphi + 0.5(C_{12}+C_{66})\sin 2\varphi)^2}}{2\rho}},$$

where φ is the angle between the *X*–axis and the direction of the AW wavevector in the *XY* plane (more generally, the angle φ is the angle between the *X*-axis and the projection of the AW wavevector on the *XY* plane.). The AW's velocities contours in the *XY* plane are presented in Fig. 1a.

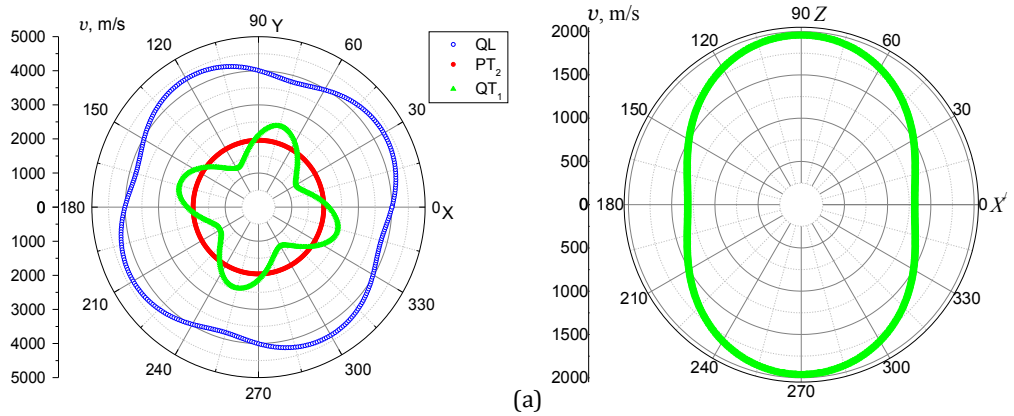


Fig. 1. (a) The AW's velocity contours in the *XY* plane (QT_1 corresponds to the quasi-transverse AW polarized in the *XY* plane, PT_2 – to the pure transverse AW polarized along the *Z* axis, and QL – quasi-longitudinal AW polarized in the *XY* plane); (b) dependence of AW QT_1 velocity on propagation direction in the $X'Z$ plane.

As can be seen, the slowest wave is the QT_1 AW, which propagates at an angle of 29 deg relative to the *X*-axis at a velocity of 1311 m/s. Thus, we will consider AO Bragg diffraction in the $X'Z$ -plane that is rotated about the *Z* axis by 29 deg. The AO interaction that will be under consideration is the anisotropic diffraction on the QT_1 AW propagated in the $X'Z$ -plane. The dependence of AW QT_1 velocity on propagation direction in the -plane is shown in Fig. 1b. The dependence of this velocity on angle θ has been obtained numerically. The geometries of the AO interaction considered in the present work are shown in Fig. 2.

The coupling relation between the diffraction angle γ and the angle between the AW wavevector and X' can be expressed in the view:

$$\theta(\gamma)=\arctan\left\{\frac{\dfrac{n_o n_e \sin(\theta_i)}{\sqrt{n_e^2\cos^2(\theta_i)+n_o^2\sin^2(\theta_i)}}-n_o\sin(\theta_i+\gamma)}{\dfrac{n_o n_e \cos(\theta_i)}{\sqrt{n_e^2\cos^2(\theta_i)+n_o^2\sin^2(\theta_i)}}-n_o\cos(\theta_i+\gamma)}\right\}, \tag{4}$$

The dependence of $\theta(\gamma)$ is presented in Fig. 3a. The angle of orientation of the AW wavevector

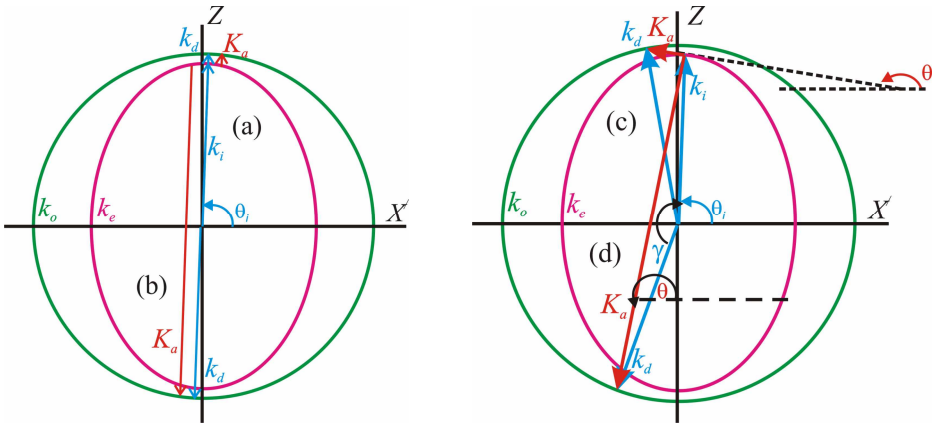


Fig. 2. The geometries of the AO interaction in $PbMoO_4$ crystals for collinear (a,b) and tangential (c,d), forward (a,c), and backward (b,d) diffractions. k_o and k_e are the wavevectors of ordinary, and extraordinary waves, respectively; k_i, k_d, and K_a are the wavevectors of incident, diffracted, and acoustic waves, respectively; γ is the angle of diffraction, θ_i is the angle between the wavevector of the incident optical wave and X' axis, and θ is the angle between the AW wavevector and X' - axis.

varies linearly with the diffraction angle, except in the range near the collinear diffraction.

To find the relations for the components of the deformation tensor caused by the AWs, we consider the Christoffel tensor components for AWs propagating at angles φ and θ. The components of the Christoffel tensor can be written as:

$$\begin{aligned}
M_{11} &= C_{11}\cos^2\theta\cos^2\varphi + C_{66}\cos^2\theta\sin^2\varphi + C_{44}\sin^2\theta + C_{16}\cos^2\theta\sin 2\varphi \\
M_{22} &= C_{66}\cos^2\theta\cos^2\varphi + C_{11}\cos^2\theta\sin^2\varphi + C_{44}\sin^2\theta - C_{16}\cos^2\theta\sin 2\varphi \\
M_{33} &= C_{44}\cos^2\theta + C_{33}\sin^2\theta \\
M_{23} &= (C_{13} + C_{44})\cos\theta\sin\theta\sin\varphi \\
M_{13} &= (C_{13} + C_{44})\cos\theta\sin\theta\cos\varphi \\
M_{12} &= C_{16}\cos^2\theta\cos^2\varphi - C_{16}\cos^2\theta\sin^2\varphi + (C_{12} + C_{66})\cos^2\theta\sin 2\varphi.
\end{aligned} \tag{5}$$

The Eqs. (5) yield the eigenvalues λ and eigenvectors n_i, n_j of the Christoffel tensor due to the relation $M_{ij}n_j = \lambda n_i$ [11]. Let us define the angles of orientation of the displacement vector of the QT_1 AW as:

$$\varphi_{dis} = \arctan(u_1/u_2), \quad \theta_{dis} = \arccos(u_3), \tag{6}$$

where u_1, u_2, and u_3 are the projections of the unit displacement vector on the coordinate axes *X, Y, Z* written as:

$$u_1 = u\cos\varphi_{dis}\cos\theta_{dis}, u_2 = u\sin\varphi_{dis}\cos\theta_{dis}, u_3 = \sin\theta_{dis}, \tag{7}$$

where u is the unit displacement vector. The dependencies of θ_{dis} and φ_{dis} on the diffraction angle γ are presented in Fig. 3b. The angle θ_{dis} of the displacement vector orientation does not depend on the diffraction angle γ and lies close to the *XY* plane. The angle φ_{dis} is independent of angle γ in the range of 90-270 deg, too, and is close to 30 deg.

Therefore, the symmetric deformation tensor components, caused by the QT_1 AW, determined as $e_{ii} = \partial u_i / \partial x_i$ and $e_{ij} = (\partial u_i / \partial x_j + \partial u_j / \partial x_i)/2$ (x_i, x_j are the *X*, *Y*, *Z* coordinates) are as follows:

$$\begin{aligned}
e_{11} &= e_0\cos\varphi_{dis}\cos\theta_{dis}, & e_{12} &= e_0\sin\varphi_{dis}\cos\theta_{dis}, \\
e_{22} &= e_0\tan\varphi_{dis}\sin\varphi_{dis}\cos\theta_{dis}, & e_{13} &= e_0\sin\theta_{dis}, \\
e_{33} &= e_0\frac{\tan\theta_{dis}\sin\theta_{dis}}{\cos\varphi_{dis}}, & e_{23} &= e_0\tan\varphi_{dis}\sin\theta_{dis},
\end{aligned} \tag{7}$$

where e_0 is the unit deformation, i.e., $e_0 = \partial u / \partial X$. The electric field of the diffracted optical wave can be written as

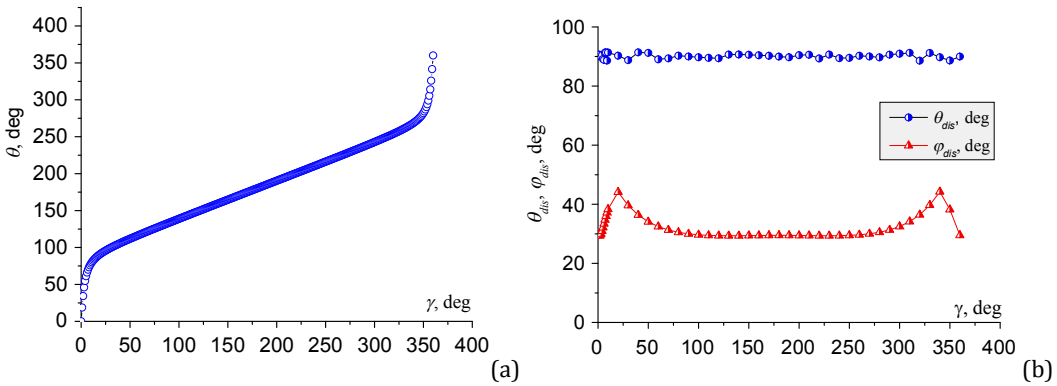


Fig. 3. Dependencies of θ angle (a) and θ_{dis} and φ_{dis} angles (b) on the diffraction angle γ.

$$E_1 = (\Delta B_{11}\cos\varphi + \Delta B_{12}\sin\varphi - \chi(\Delta B_{11}\sin\varphi - \Delta B_{12}\cos\varphi))D_0$$
$$E_2 = (\Delta B_{21}\cos\varphi + \Delta B_{22}\sin\varphi - \chi(\Delta B_{21}\sin\varphi - \Delta B_{22}\cos\varphi))D_0, \quad (8)$$

where D_0 is a unit vector of the electric induction of the incident optical wave, E_i are the components of the electric field of the diffracted optical wave, ΔB_{ji} is the increment of the impermeability tensor due to the deformations caused by AW, χ is the ellipticity of the incident and one of the eigen optical waves, and $\theta_i = 89.9$ deg is the angle between X' axis and the wavevector of the incident optical wave. From Eqs. (7), one can find the magnitude of the electric field vector of the diffracted optical wave:

$$E = \sqrt{E_1^2 + E_2^2}\,. \quad (9)$$

and then the relation for the effective EO coefficient. This relation is not presented here because it is quite cumbersome and can be evaluated only numerically.

The ellipticities of optical eigenwaves induced by the electro-gyration and Faraday effect are as follows

$$\chi(\theta_i) = \frac{1}{2\beta_{33}E_3}\left[n_o^2 - n_e^{2*} - \sqrt{(n_o^2 - n_e^{2*})^2 + 4\beta_{33}^2E_3^2}\right], \quad (10)$$

$$\chi(\theta_i) = \frac{1}{2\alpha_{33}H_3}\left[n_o^2 - n_e^{2*} - \sqrt{(n_o^2 - n_e^{2*})^2 + 4\alpha_{33}^2H_3^2}\right], \quad (11)$$

respectively. In the Eqs. (10,11) $\alpha_{33} = 0.96\times10^{-12}$ rad×m/A, and

$$n_e^* = \frac{n_o n_e}{\sqrt{n_e^2\sin^2(\theta_i) + n_o^2\cos^2(\theta_i)}}\,. \quad (12)$$

3. Results and discussion

Fig. 4 shows the dependence of the effective EO coefficient (Fig. 4a) and the AO figure of merit (Fig. 4b) on the diffraction angle under the application of the bias field E_3^0. The angle of incidence of the optical wave remains unchanged and is equal to $\theta_i = 89.9$ deg. The effective EO coefficient and the AO figure of merit both increase as the electric field strength grows. The behavior of the AO figure of merit and the ellipticity of the eigen optical wave corresponding to the incident optical wave on the electric field (Fig. 5) is the same; i.e., both parameters increase sharply with the electric field and then saturate at about 20×10^6 V/m.

The ellipticity close to unity, corresponding to an almost circularly polarized optical wave, is reached at a relatively high electric field of 10^8 V/m. Fig. 5a,b depicts the dependence of the AO figure of merit for $\gamma = 0$ (for forward collinear AO diffraction (Fig. 2a)) and 160 deg (for backward tangential AO diffraction (Fig. 2d)) on electric field. The dependence of ellipticity of eigen waves on the electric field is presented in Fig. 5c. As one can see, the AO figure of merit increases from 2.8×10^{-15} s^3/kg at zero electric field and zero ellipticity of the eigen wave to 7.1×10^{-15} s^3/kg at 10^7 V/m and an ellipticity of 0.9 for the case of forward collinear AO diffraction (Fig. 5a,c). It should be noted that the conditions of our simulation correspond to the incidence of an optical wave close to the optical axis, where the linear birefringence is small, equal to 4.1×10^{-7}. At an incidence angle far from the optical axis, the condition of achieving an ellipticity close to unity can be met at sufficiently high electric fields that threaten electrical breakdown of the crystal. On the other hand, the small elliptical birefringence in the direction of the incident optical wave propagation leads to the phase-matching conditions that are satisfied at low AW frequency

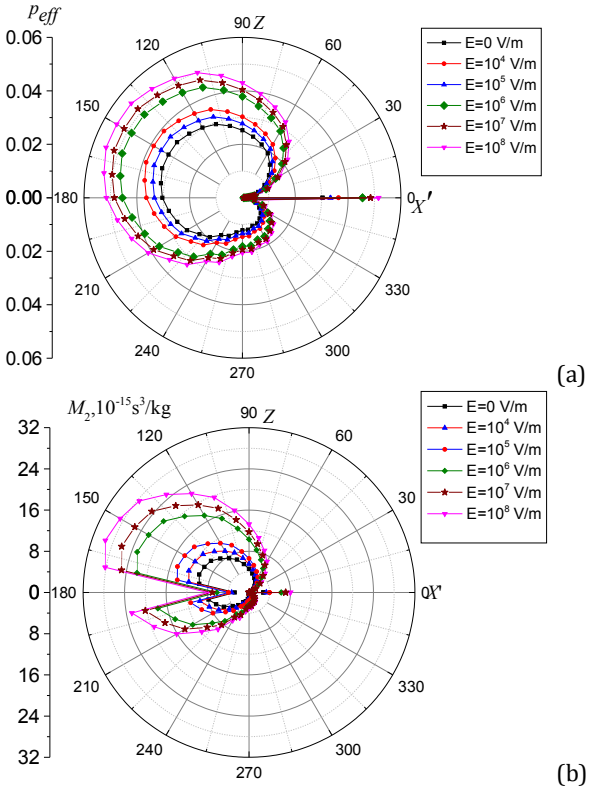


Fig. 4. Dependencies of the effective EO coefficient (a) and AO figure of merit (b) on the diffraction angle under the applied electric field E_3^0.

(15.08 kHz) and long wavelength of AW (0.13 m). Under these conditions, collinear diffraction cannot be achieved in crystals of realistic size. At backward collinear diffraction, one can achieve an AO figure of merit of 6.2×10^{-15} s^3/kg even at E_3^0=10^6 V/m. However, in this case, the AW frequency is extremely high (14 GHz), which is difficult to reach in bulk AO devices.

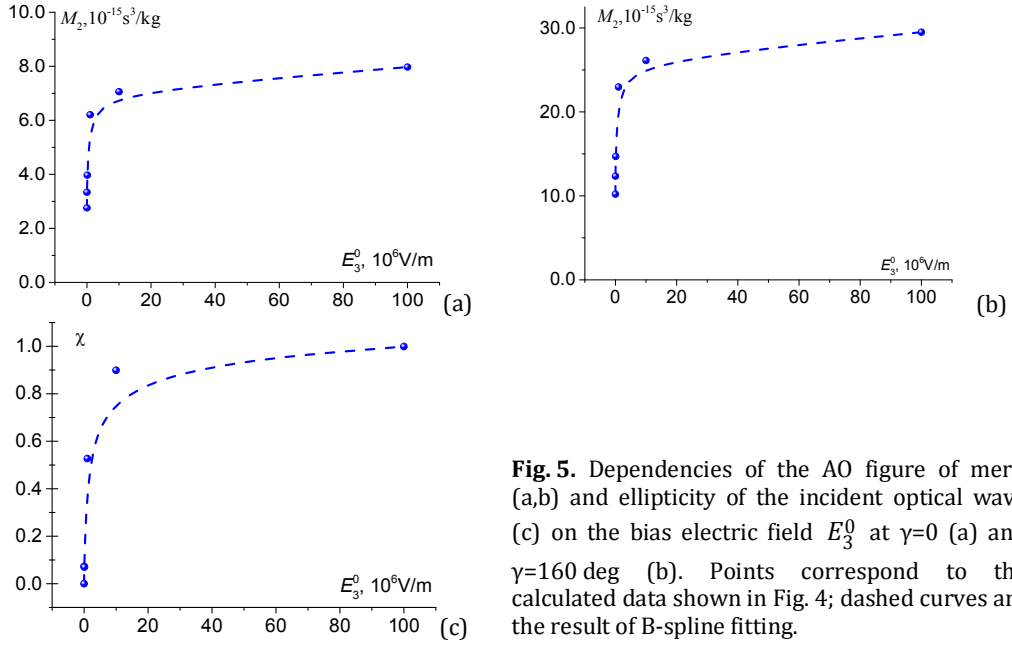
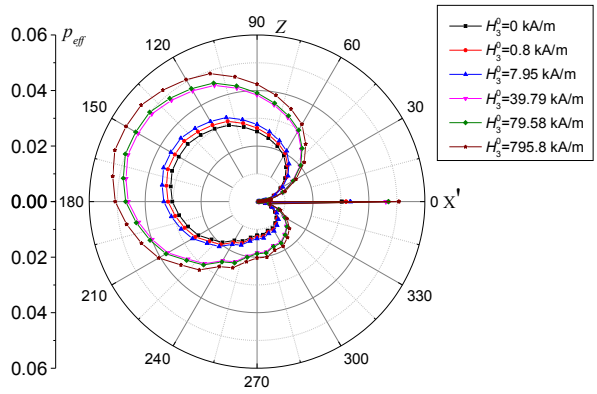


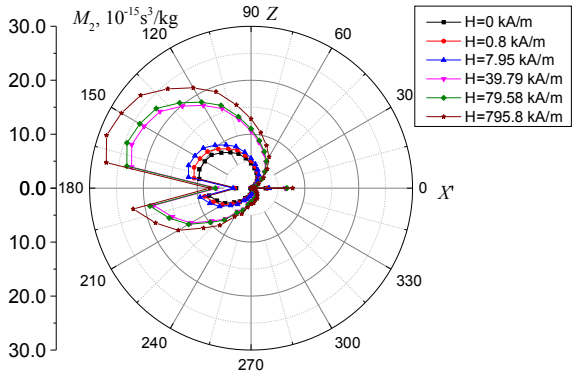
Fig. 5. Dependencies of the AO figure of merit (a,b) and ellipticity of the incident optical wave (c) on the bias electric field E_3^0 at γ=0 (a) and γ=160 deg (b). Points correspond to the calculated data shown in Fig. 4; dashed curves are the result of B-spline fitting.

The AO figure of merit for tangential Bragg diffraction at the diffraction angle $0<\gamma\leq10$ deg (Fig. 2c), corresponding to the frequency range of AW 96 MHz$<\Omega\leq$1.0 GHz, is quite small (Fig. 4b), not exceeding 0.17×10^{-15} s^3/kg even at an electric field strength of 10^8 V/m. The highest AO figure of merit (29×10^{-15} s^3/kg) is reached at γ=160 deg and $E_3^0=10^8$ V/m, i.e., backward tangential diffraction (Fig. 2d). Even at $E_3^0=10^6$ V/m, the AO figure of merit is sufficiently high (23×10^{-15} s^3/kg) (see Fig. 5b). This value corresponds to the ellipticity of the eigenwaves equal to χ=0.53 (Fig. 5c). However, the AW frequency remains high under this condition (9.8 GHz). It should be noted that AW frequencies such as 14 and 9.8 GHz are too high for the bulk AO cells. Nonetheless, this frequency range is available for integrated-optic AO devices [25-27].

The dependence of the effective EO coefficient and the AO figure of merit on the diffraction angle at different applied magnetic field values, H_3^0, is shown in Figs. 6a and 6b. These dependencies are similar to those considered above for the electric-field case.



(a)



(b)

Fig. 6. Dependencies of the effective EO coefficient (a) and AO figure of merit (b) on the diffraction angle under the applied magnetic field H_3^0.

The same is true for the dependencies of the AO figure of merit and the ellipticity of the eigenwave on the magnetic field (Fig. 7a-c).

The highest AO figure of merit is reached at γ=160 deg. At H_3^0=37.5 kA/m, the AO figure of merit is equal to 23×10^{-15} s^3/kg. This value corresponds to the ellipticity of the eigenwaves, equal to χ=0.53. By considering the energy densities of the electric and magnetic fields

$$W_E=\frac{1}{2}\varepsilon_r\varepsilon_0(E_3^0)^2 \text{ and } W_H=\frac{1}{2}\mu\mu_0(H_3^0)^2, \quad (13)$$

($\varepsilon_r = 40$ at the frequency of the electric field 10 Hz and temperature 390 K [23], $\varepsilon_0 = 8.854\times10^{-12}$ F/m, $\mu = 1$ and $\mu_0 = 1.257\times10^{-6}$N/A^2) required to achieve an AO figure of merit of 23×10^{-15} s^3/kg, one can compare them to determine which field is energetically preferable. Here, the energetic preference means the determination of the part of energy that is needed for inducing the optical activity by an electric or magnetic field, then increasing the AO figure of merit, and finally increasing the efficiency of AO diffraction. The energetic losses of different types are not considered. It has been found that W_E=1.77×10^2 J/m^3 while W_H=8.83×10^2 J/m^3. Therefore, applying an electric field requires an energy density sufficiently lower than that of a magnetic field to achieve the same conditions (M_2 = 23×10^{-15} s^3/kg). It should be noted that applying both fields with the specified values to achieve the corresponding energy densities is technically feasible and does not require expensive technology.

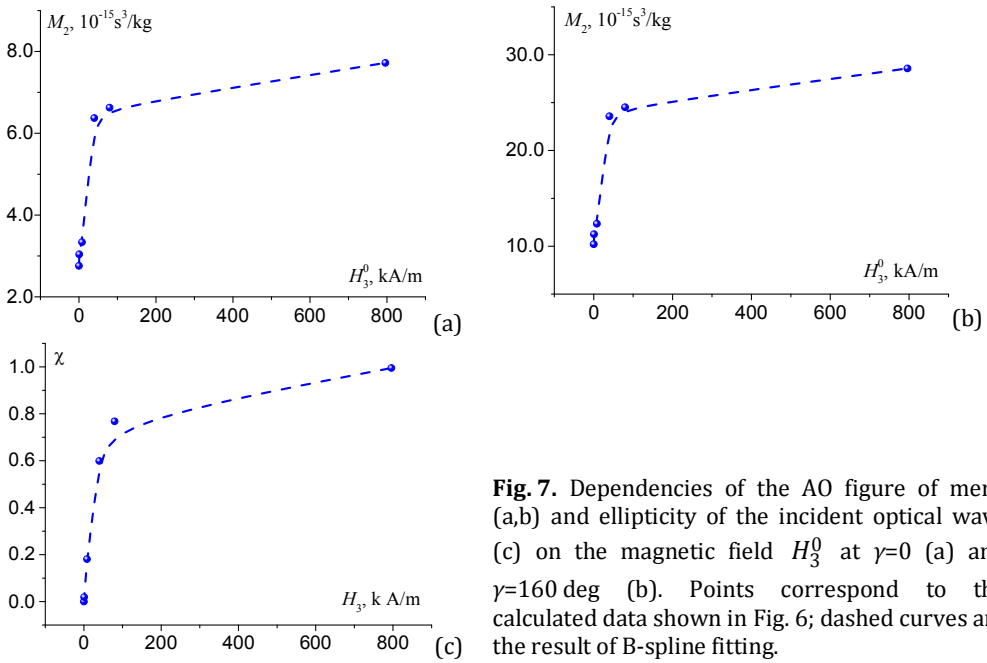


Fig. 7. Dependencies of the AO figure of merit (a,b) and ellipticity of the incident optical wave (c) on the magnetic field H_3^0 at γ=0 (a) and γ=160 deg (b). Points correspond to the calculated data shown in Fig. 6; dashed curves are the result of B-spline fitting.

Now let us determine the AW energy density that is required for reaching M_2=10^{-14} s^3/kg at E_3^0=0 V/m and 23×10^{-15} s^3/kg at E_3^0 =10^6 V/m (γ=160 deg). By the same values, the AO figure of merit correspond to magnetic field strengths of 0 and H_3^0=37.5 kA/m. Let us use Eq. (1) and the following parameters: l=b=10^{-2} m; the AW velocity v_{QT_1} =1820 m/s; the Bragg angle is $\theta_B = 80$ deg; the diffraction angle is equal to 160 deg, and the efficiency of diffraction is assumed to be equal η=0.1; here and above, the size of the AO cell is accepted to be equal 1×1×1 cm^3. The AW velocity of 1820 m/s corresponds to AW propagation at an angle of θ = 240 deg. At the small AO diffraction efficiency, Eq. (1) can be rewritten as:

$$\eta \approx \frac{\pi^2 l}{2\lambda^2 b\cos^2\theta_B} M_2 P_a . \qquad (14)$$

Under our parameters, the relation $\pi^2 l/2\lambda^2 b\cos^2\theta_B$ is equal to 411.8×10^{12} m^{-2}. In order to reach AO efficiency equal to 0.1 at AO figure of merit 10^{-14} s^3/kg one has to excite the AW with the acoustic power equal to P_a=2.4×10^{-2} W. The AW power density is defined as [28]:

$$\frac{P_a}{lb}=\frac{1}{2}\rho v_{QT_1}^3 e_{ij}^2=W_a v_{QT_1}. \quad (15)$$

Therefore, the corresponding energy density $W_a = P_a / lbv_{QT_1} = 13.2\times10^{-2}$ J/m^3. Without increasing the AO figure of merit to 23×10^{-15} s^3/kg, one has to increase the AW power by 2.3 times, i.e., to P_a = 5.52×10^{-2} W, and the AW energy density to 30.36×10^{-2} J/m^3. The difference between the AW energy densities is equal to 0.17 J/m^3. As one can see, the energy density that is needed to increase the efficiency of AO diffraction by 2.3 times with the help of increasing the power of AW is three to four orders of magnitude lower than the energy density of the electric or magnetic field, respectively used for the same aim. However, when smaller values of the geometric parameters l and b are required, the energy density of AW can become comparable to that of the electric and magnetic fields. It should be noted that the above energetic calculations are valid only for $PbMoO_4$ crystals in a certain geometry of AO interaction and electric and magnetic field application. Other crystalline materials are characterized by their constitutive coefficients; therefore, the relationship among W_E, W_H, and W_a can differ.

4. Conclusions

In the present work, we have considered the influence of electric and magnetic fields on the AO figure of merit in $PbMoO_4$ crystals, arising from electro-gyration and Faraday effects that induce elliptical birefringence. The analysis was performed for the case of anisotropic AO interaction with the slowest AW QT_1, propagated in the $X'Z$ plane that was rotated by 29° around the Z-axis. The incident optical wave propagated almost along the Z-axis (the angle between the Z-axis and the incident wave wavevector was 0.1 deg). Several types of AO interactions have been considered, i.e., collinear forward and backward AO diffraction and tangential forward and backward AO diffraction. The ellipticity of the incident optical wave induced by electric and magnetic fields was taken into consideration. It has been found that in all mentioned cases the action of the electric and magnetic field leads to an increasing in the AO figure of merit. For the case of forward collinear diffraction, the AO figure of merit increases from 2.8×10^{-15} s^3/kg at zero electric field and zero ellipticity of the eigen wave to 7.1×10^{-15} s^3/kg at 10^7 V/m and an ellipticity of 0.9. The same is true for the magnetic fields 0 and 795.8 kA/m, respectively. However, the small elliptical birefringence in the direction of the incident optical wave propagation leads to the phase-matching conditions that are satisfied at low AW frequency (15.08 kHz) and long wavelength of AW (0.13 m). Under these conditions, the forward collinear diffraction cannot be achieved in crystals of realistic size. At backward collinear diffraction, one can achieve an AO figure of merit of 6.2×10^{-15} s^3/kg at E_3^0 =10^6 V/m (or magnetic field H_3^0 =37.5 kA/m). Although the AO figure of merit increases by about a factor of 3 under electric or magnetic field conditions, the AW frequency in this case is extremely high (14 GHz), which is difficult to achieve. The AO figure of merit for the forward tangential Bragg diffraction at the diffraction angle $0<\gamma\leq10$ deg corresponding to the frequency range of AW 96 MHz$<\Omega\leq$1.0 GHz is quite small, not exceeding 0.17×10^{-15} s^3/kg even at an electric field strength of 10^8 V/m or magnetic field 795.8 kA/m. The highest AO figure of merit (29×10^{-15} s^3/kg) is reached at γ=160 deg and E_3^0 =10^8 V/m (or magnetic field 795.8 kA/m), i.e. at the backward tangential AO diffraction. Even at E_3^0 =10^6 V/m (or magnetic field 37.5 kA/m),

the AO figure of merit is sufficiently high (23×10^{-15} s^3/kg). This value corresponds to the ellipticity of the eigenwaves equal to χ=0.53 and the AW frequency of 9.8 GHz. The AO figure of merit increases by a factor of 2.3 under electric or magnetic field application.

In the last case of AO diffraction, we have carried out a comparative analysis of the energy densities of the electric and magnetic fields required to enhance AO diffraction efficiency to a certain level by increasing the AO figure of merit and the energy density of AW, which is necessary to achieve this AO efficiency without applying an electric or magnetic field. With the chosen parameters, the electric and magnetic field energy densities are three to four orders of magnitude higher than those of the AW. However, AO diffraction is a complex process. For example, increasing the AW power can introduce nonlinearities in AO diffraction or produce additional diffraction orders. Moreover, the AW energy density depends on the acoustic beam's (or piezoelectric transducer's) geometric parameters. Decreasing these parameters can equalize the energy densities of the magnetic or electric fields and the AW.

Funding. This work was supported by the Ministry of Education and Science of Ukraine (project #0125U002027) and the National Research Foundation of Ukraine (project # 0126U003340 "Revealing and systemic study of the effects of parametric crystal acoustics").

Conflict of interest. Authors declare no conflict of interest.

Authors' contributions. Mys O.- computer simulation, data processing, project funding; Kostyrko M. – results analysis, paper correction; Skab I. – results analysis, paper correction; Vlokh R. – study aim formulation, results analysis, paper writing; project funding.

References

1. Brillouin, L. (1922). Diffusion de la lumière et des rayons X par un corps transparent homogène. Influence de l'agitation thermique. *Annales de Physique, 9*, 88–122.
2. Debye, P., & Sears, F. W. (1932). On the scattering of light by supersonic waves. *Proceedings of the National Academy of Sciences, 18*, 409–414.
3. Lucas, R., & Biquard, P. (1932). Optical properties of solid and liquid media subjected to high-frequency elastic vibrations. *Journal de Physique, 71*, 464–471.
4. Vlokh, O. G. (1984). *Spatial dispersion phenomena in parametrical crystal optics*. Vyshcha Shkola.
5. Ling, B., Dennis, G. I., Miller, H. M., Spaine, T. W., & Carnahan, J. W. (2004). Acousto-optic tunable filters: Fundamentals and applications as applied to chemical analysis techniques. *Progress in Quantum Electronics, 28*, 67–87.
6. Magdich, L. N., & Molchanov, V. Ya. (1989). *Acoustooptic devices and their applications*. Gordon and Breach Science Publishers.
7. Pichugina, Y. V., Nosov, P. A., Batshev, V. I., Machikhin, A. S., Kozlov, A. B., & Krasin, G. K. (2019). 3D manipulation of micro-objects based on optical tweezers using acousto-optic deflector and variofocal system. *Proceedings of SPIE, 11060*, 110601A-1–110601A-7.
8. Lim, S., Baek, S., Whitlow, J., D'Onofrio, M., Chen, T., Phiri, S., Crain, S., Brown, K. R., Kim, J., & Kim, J. (2025). Design and characterization of individual addressing optics based on multi-channel acousto-optic modulator for $^{171}Yb^+$ qubits. *Optics & Laser Technology, 180*, 111436.
9. Martynyuk-Lototska, I., Vasylkiv, Y., Dudok, T., Skab, I., & Vlokh, R. (2018). Acoustooptic operation of optical vortex beams. *Optik, 155*, 179–184.
10. Tang, Y., Burdick, N. Q., Baumann, K., & Lev, B. L. (2015). Bose–Einstein condensation of ^{162}Dy and ^{160}Dy. *New Journal of Physics, 17*(4), 045006.
11. Sirotin, Yu. I., & Shaskolskaya, M. P. (1982). *Fundamentals of crystal physics*. Mir Publishers.
12. Cook, W. R., Nelson, D. F., & Vedam, K. (1996). *Piezooptic and electrooptic constants*. Landolt-Börnstein: Numerical Data and Functional Relationships in Science and Technology, New Series, Vol. 30A.
13. Yano, T., & Watanabe, A. (1974). Acousto-optic figure of merit of TeO_2 for circularly polarized light. *Journal of Applied Physics, 45*, 1243–1245.
14. Mys, O., Kostyrko, M., Adamenko, D., Martynyuk-Lototska, I., Skab, I., & Vlokh, R. (2022). Effect of ellipticity of optical eigenwaves on the enhancement of efficiency of acousto-optic Bragg diffraction: A case of optically active $Pb_5Ge_3O_{11}$ crystals. *AIP Advances, 12*(5), 055130.
15. Krupych, O., Mys, O., Dudok, T., Say, A., & Vlokh, R. (2025). Effect of polarization ellipticity of the incident optical wave on acousto-optic diffraction efficiency and intensity modulation: Case of TeO_2 crystals. *Applied Optics, 64*, 8308–8313.

16. Mys, O., Adamenko, D., & Vlokh, R. (2024). Enhancement of the efficiency of acousto-optic diffraction due to the ellipticity of eigen optical waves caused by the electro-gyration effect in lead germanate crystals. *Ukrainian Journal of Physical Optics, 25*, 03001–03012.
17. Mys, O., Kostyrko, M., & Vlokh, R. (2025). Effect of magnetic field on the efficiency of isotropic acousto-optic diffraction in optically resistant β-BaB_2O_4 crystals. *Ukrainian Journal of Physical Optics, 26*, 01023–01031.
18. Mys, O., Adamenko, D., Kostyrko, M., & Vlokh, R. (2025). Effect of magnetic field on the acousto-optic diffraction efficiency in $NaBi(MoO_4)_2$ crystals. *Ukrainian Journal of Physical Optics, 26*(3), 03057–03066.
19. Li, C. (2016). Magnetooptic sensor based on electrogyration compensation for Faraday effect in lead molybdate crystal. *IEEE Sensors Journal, 16*(9).
20. Vlokh, O. G., Zheludev, I. S., & Klimov, I. M. (1975). Optical activity of the centrosymmetric crystals of lead molybdate ($PbMoO_4$), induced by electric field (electrogyration). *Doklady Akademii Nauk SSSR, 223*(6), 1391–1392.
21. Li, C., Song, N., & Zhang, C. (2015). Verdet constant measurements of β-barium borate and lead molybdate crystals. *Optical Materials Express, 5*(9), 1991–1997.
22. Leciejewicz, J. (1965). A neutron crystallographic investigation of lead molybdenum oxide, $PbMoO_4$. *Zeitschrift für Kristallographie – Crystalline Materials, 121*(1–6), 158–164.
23. Piwowarska, D., Kaczmarek, S. M., & Berkowski, M. (2008). Dielectric, optical and EPR studies of $PbMoO_4$ single crystals, pure and doped with cobalt ions. *Journal of Non-Crystalline Solids, 354*, 4437–4442.
24. Coquin, G. A., Pinnow, D. A., & Warner, A. W. (1971). Physical properties of lead molybdate relevant to acousto-optic device applications. *Journal of Applied Physics, 42*, 2162.
25. Shao, L., Sinclair, N., Leatham, J., Hu, Y., Yu, M., Turpin, T., Crowe, D., & Lončar, M. (2020). Integrated microwave acousto-optic frequency shifter on thin-film lithium niobate. *Optics Express, 28*(16), 23728–23738.
26. Li, H., Liu, Q., & Li, M. (2019a). Electromechanical Brillouin scattering in integrated planar photonics. *APL Photonics, 4*, 080802.
27. Liu, Q., Li, H., & Li, M. (2019b). Electromechanical Brillouin scattering in integrated optomechanical waveguides. *Optica, 6*(6), 778–785.
28. Balakshiy, V. I., Parygin, V. N., & Chirkov, L. E. (1985). *Physical principles of acousto-optics*. Radio i Svyaz.

Mys, O., Kostyrko, M., Skab, I., Vlokh, R. (2027). Energy-Efficiency Comparison of Electric- and Magnetic-Field Enhancement of Acousto-Optic Diffraction in $PbMoO_4$ Crystals. *Ukrainian Journal of Physical Optics*, *28*(1), 01077 – 01088.
doi: 0.3116/16091833/Ukr.J.Phys.Opt.2027.01077

Анотація. *У роботі розглядається вплив електричного і магнітного поля на коефіцієнт акустооптичної (АО) якості в кристалах $PbMoO_4$, зумовлений ефектами електрогірації та Фарадея, які викликають еліптичне подвійне променезаломлення. Проаналізовано кілька типів анізотропних АО-взаємодій за участю найповільнішої акустичної хвилі QT_1: колінеарну АО-дифракцію (у прямому та зворотному напрямках) і тангенціальну АО-дифракцію (у прямому та зворотному напрямках). Найвищого значення коефіцієнта АО якості (29×10^{-15} $с^3/кг$) досягнуто у випадку зворотної* тангенціальної АО-дифракції при *$E=10^8$ В/м (або магнітному полі 795,8 кА/м). Встановлено, що навіть при напруженості електричного поля $E_3 = 10^6$ В/м (або напруженості магнітного поля 37,5 кА/м) коефіцієнт АО якості зростає до 23×10^{-15} $с^3/кг$; тобто під дією електричного або магнітного поля він зростає у 2,3 раза. Для цього типу АО-дифракції проведено порівняльний аналіз густин енергії електричного та магнітного полів, необхідних для підвищення ефективності АО-дифракції до певного рівня (шляхом збільшення коефіцієнта АО якості), та потужності акустичної хвилі, необхідної для досягнення такої ж ефективності за відсутності зовнішніх електричних чи магнітних полів. Виявлено, що за обраних параметрів, густини енергії електричного та магнітного полів значно перевищують густину енергії акустичної хвилі. Проте, існує чимало умов, за яких ці густини енергії можуть зрівнятися.*

Ключові слова: *акустооптична дифракція, електрогірація, ефект Фарадея, акустооптична ефективність, густина енергії*